Transactions, SMiRT-26
Berlin/Potsdam, Germany, July 10-15, 2022
Special Session: Performance assessment of spent fuel in storage and transportation

SPENT NUCLEAR FUEL AND CANISTER TEMPERATURE PREDICTION DURING TRANSFER, STORAGE, AND SEVERE FIRE ACCIDENT CONDITIONS

Megan Higley[1], Mustafa Hadj-Nacer[1], Ahti Suo-Anttila[3], and Miles Greiner[4]

[1] Research Assistant, University of Nevada, Reno, Reno, Reno, Nevada, USA
[2] Research Assistant Professor, University of Nevada, Reno, Reno, Nevada, USA
[3] Principal, Computational Engineering Analysis LLC, Albuquerque, New Mexico, USA
[4] Professor, University of Nevada, Reno, Reno, Nevada, USA (greiner@unr.edu)

ABSTRACT

Since 1993, researchers from the University of Nevada, Reno Nuclear Packaging Program have partnered with others to develop and experimentally validate computational fluid dynamics models to accurately predict temperatures in spent nuclear fuel (SNF) casks under normal transfer, storage, and transport operations, and in severe fire accidents. They used these methods to predict how normal-operations peak cladding and other temperatures are affected by uncontrolled internal gap dimensions and gas rarefaction. Package designers can use these methods to determine how long SNF must spend in wet storage so that components do not reach limit temperatures during normal operations. They also predicted how long a large pool fire must last before certain internal components could reach their limit temperatures, and how those durations of concern increase when the package is offset from the center of the fuel source. Transportation risk analysists can use this type of analysis to distinguish between highly unlikely fire accident scenarios that can or cannot challenge the integrity of a cask to provide its required safety functions.

INTRODUCTION

Spent Nuclear Fuel (SNF) consists of square arrays of highly radioactive heat-generating fuel pellets sealed inside thin-walled zircaloy cladding tubes [1]. After SNF is removed from a reactor, it is initially stored underwater while its heat generation and radioactivity decrease. After sufficient time, it may be moved to multi-layered casks, or stainless-steel canisters inserted in different types of overpacks, for on-site dry storage or off-site transport. To transfer the SNF, a cask, or a canister inside a transfer cask, is lowered into the pool. Both types of packages contain baskets, consisting of multiple square cross-section stainless-steel tubes, into which individual SNF assemblies are placed. The packages are then covered, lifted from the pool, and drained while helium or another inert gas flows in. The remaining moisture is then removed to reduce the likelihood of future corrosion or combustible gas formation. The package is then filled with inert dry gas, to pressures between 1 and 8 atmospheres, and sealed.

Federal regulations [2] require packaging to contain the SNF, control criticality, and shield the surroundings from radiation. Transport packages must provide these safety functions under normal conditions of transport (NCT), which includes high and low temperature environments with or without solar insolation. They must also provide these functions during hypothetical accident conditions (HAC), which consist of the following sequence: a 9-m drop onto an unyielding surface, a 1-m drop onto a puncture bar, 30-minute engulfment in an 800°C-fire, and finally, water submersion. The current absence of a national disposition plan may require that SNF be safely transported and processed after 100 years or more in dry storage.

The temperature of SNF cladding and other packaging components affect their degradation rate, physical integrity, and ability to provide their required safety functions, as well as the suitability of the SNF to be processed after storage and transport. Component temperatures must not exceed different limits that apply during NCT and HAC. Since 1993, the University of Nevada, Reno Mechanical Engineering Department's Nuclear Packaging (NP) Program has conducted research with other institutions to develop and experimentally validate computation models that predict packaging temperatures during normal transfer, storage, and transport, as well as severe fire conditions. The objective of this paper is to summarize this work in general. Specifics of this research are available in the references.

REPRESENTATIVE SNF CASKS

Industry uses a range of cask designs to transport different numbers of SNF assemblies by truck and rail. Figure 1 shows an axis-symmetric computational model of a bolted legal-weight truck cask designed to transport one spent pressurized water reactor (PWR) fuel assembly [3, 4]. In this model, the fuel assembly rods, instrument tubes, and surrounding gas are not represented explicitly. For expediency, the region containing the fuel is represented as a solid fuel block with an effective density, specific heat, and temperature-dependent effective thermal conductivity. Limits on the accuracy of using a continuum to model these discrete elements are described in the literature [5]. In Fig. 1, the fuel block is surrounded by an aluminum basket. Stainless steel inner and outer layers surround a lead gamma shield. Ethylene glycol/water mixture-filled neutron shield and overflow tanks that are stiffened with radial stainless-steel plates surround the gamma shield. The package base is stainless steel with a lead gamma shield plug. A bolted stainless-steel lid at the other end is sealed using an O-ring. The outer diameter of the cask body is approximately 1 m. Honeycomb-filled impact limiters surround both ends of the cask.

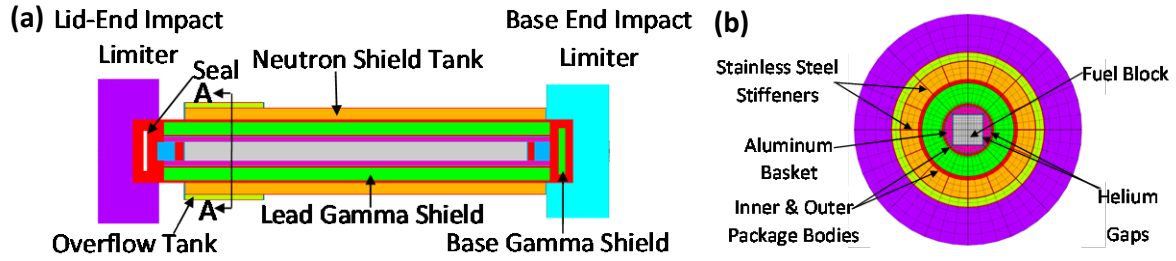

Figure 1: Computational model of a legal-weight truck cask designed to transport one pressurized water reactor spent fuel assembly [3,4]. (a) Axial section. (b) Transverse cross section view A-A as seen in part (a).

Figure 2 is two-dimensional cross-section model of a much larger SNF cask designed to transport 32 PWR assemblies by rail [6, 7]. For this helium-filled cask, each assembly is explicitly modeled as a 17×17 array of zircaloy fuel rods and hollow instrumentation tubes. The assemblies are centered within square cross-section stainless-steel basket tubes with aluminum and Boral plates bonded to their surfaces. A thin stainless-steel skin wraps around the basket. Aluminum rails that are between the flat outer surfaces of the basket and the round stainless-steel containment boundary are also included. Outside the containment boundary are a carbon-steel gamma shield, a polymer neutron shield stiffened by radial aluminum plates, and a stainless-steel outer shell. The outer diameter of the rail cask is approximately 2.5 m. Figure 1b shows the details of a portion of the cross-section, including small gaps between the basket and rails. Those gaps facilitate cask assembly, manufacturing tolerances, and allow for thermal expansion without causing excessive strain. If the basket is centered within the package, the nominal basket/rail gap width at all locations is W = 4.78 mm. However, if there is differential thermal expansion, shifting, or leaning of the

basket, the gap width may be smaller and/or non-uniform. As a result, the basket/rail gap size and uniformity inside a loaded sealed cask are not precisely controlled or known.

While many components many are important to package performance, in this work we focus on predicting the maximum or peak cladding temperature, T_{PC}, to assure it does not exceed specified limits during normal or fire conditions [8]. For example, to assure that SNF may be safely transported and processed after drying and long-term storage, T_{PC} for zircaloy cladding must not exceed certain limits (that depend on several factors but are around 400°C) during all post-reactor operations to avoid radial hydride formation, which may embrittle the cladding and make future processing more difficult. During and after fire accident conditions, the ability of the fuel cladding to contain the fuel may be reduced if T_{PC} exceeds its burst rupture temperature, $T_{BR} = 750^oC$ [27]. Package system employs several layers of containment. As a result, they are designed to continue to provide their safety functions even if T_{PC} exceeds these limits under either circumstance.

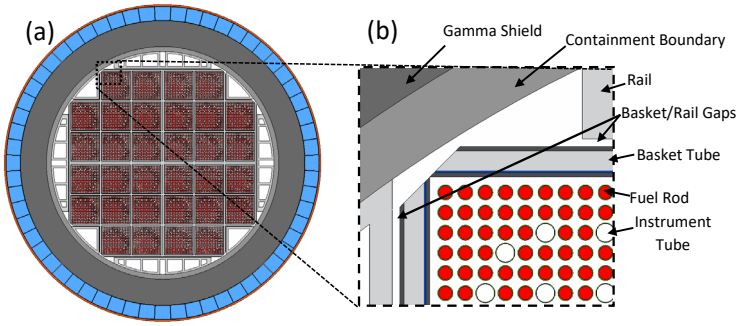

Figure 2 Geometrically accurate SNF rail cask cross-section (a) Full cross section. (b) Detail.

SNF DRYING, STORAGE, AND TRANSPORT MODEL DEVELOPMENT

To assure package component temperatures do not exceed their limits, it is important to accurately model package conduction, convection, and radiation heat transfer, and their uncertainties under normal (transfer, storage, and transport) and fire accident conditions. After SNF is loaded into casks or canisters and the water is drained, most of the remaining moisture is removed, by either vacuum drying or forced helium dehydration [9]. In vacuum drying, the gas is evacuated in stages to pressures as low as 70 Pa to promote evaporation and vapor removal. At these low pressures, the mean free path between molecular collisions λ increases and begins to approach the width W of the small passages within the cask. For $0.001 < \lambda/W < 0.1$, the gas is in the slip-flow rarefied gas regime [10]. In this regime, a conduction thermal resistance develops at the interfaces between solid surfaces and the gas [11]. This resistance is negligible in the continuum regime. Fuel drying is the first operation when the SNF is not in a water-cooled environment, and it heat generation rate is still relatively high. As a result, the hottest T_{PC} may occur during that operation. We focus on vacuum drying because the thermal resistance it introduces increases package component temperatures compared to drying methods in which the gas remains in the continuum regime.

For the rail cask in Fig. 2, there are solid/gas interfaces at the surfaces of the fuel rods, basket tubes, and basket/rail gaps. The heat flux from individual fuel rods is relatively low and their temperatures are relatively high. As a result, most of the heat is transferred across the gas between the fuel rods and basket surfaces by radiation. Any reduced gas conduction in this region does not strongly affect the peak cladding or other temperatures. However, under steady state conditions nearly all heat generated by the SNF flows across the basket/rail gaps. As a result, any thermal resistance across those gaps causes large temperature differences compared to other package components. Moreover, the gap surfaces are relatively cool because they are near the package parameter, and so radiation heat transfer across the gaps is small compared to conduction [10]. The conduction thermal resistance and temperature difference across the gap are relatively large and strongly dependent on the gap width, whose value, as described earlier, is not precisely controlled.

When predicting peak cladding and other temperatures, it is therefore important to perform thermal simulations for a range possible of basket/rail gap configurations, with and without rarefaction, to determine how they may affect package temperatures.

In the next subsection, we describe an experiment that simulates a SNF assembly within a square cross-section basket tube under normal drying, storage, and transport conditions. We use it to measure the effect of rarefaction and radiation heat transfer. We then use those data to validate computational fluid dynamics (CFD) methods that model conduction (including gas rarefaction), natural convection, and radiation heat transfer in that configuration.

Experimental Measurement Figure 3 is a drawing of the validation experimental apparatus that the NP Program constructed [12]. It consists of a 7×7 array of rods, each containing an electrical heater element along its length, and one thermocouple. The rods are held in place by top and bottom spacer plates. Support bars connect the plates to a helium-filled square cross-section stainless-steel pressure vessel. The rods are centered with in vessel and are aligned with gravity. The origin of the vertical z-coordinate is at the heater array and enclosure mid-height. The thermocouples in different rods are near $z = 0, \pm 10,$ or ± 25 cm. Heater power and thermocouple connections pass through the vessel's top and bottom flanges. Tubing and gages connected to the bottom flange allow the vessel to be filled with dry helium or other gases for a range of pressures. Thermocouples measure the outer surface temperatures of the four vessel walls and the spacer plates. Fiberboard insulation, with thicknesses of either I = 2.5 or 5.2 cm, is fastened to the vessel's outer surface to increase the experiment temperature compared to no insulation. Based on the minimum spacing between rod surfaces, this the helium gas enters the slip-flow rarefied gas regime when the pressure is below P < 5000 Pa.

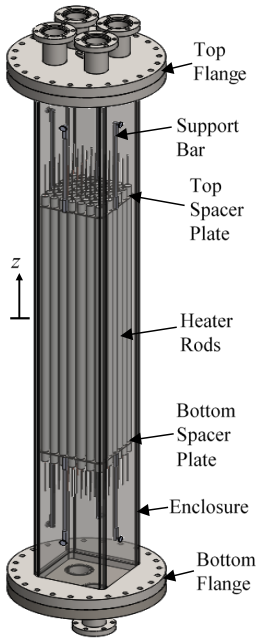

Figure 3 An experimental apparatus that models the thermal conditions of a SNF assembly within a square-cross section basket tube.

The symbols and bars in Figure 4 show the measured mid-height temperature difference $\overline{\Delta T}_{mid}$ and its uncertainty versus helium pressure P. $\overline{\Delta T}_{mid}$ is the difference between the average temperature of four central rods whose temperatures are measured near $z = 0$ and the average mid-height enclosure temperature. Figure 4 presents results for three total rod heat generation rates, Q = 50, 100, and 150 W, and two insulation thicknesses, I = 2.5 cm (open symbols) and 5.1 cm (filled symbols). For a given system pressure, $\overline{\Delta T}_{mid}$ increases with Q, as expected. For a given pressure and heat generation rate, Fig. 4 shows that the temperature difference decreases as when the insulation thickness increases. This is because increasing the insulation thickness increases the system temperatures, which increases heat transported by radiation. Finally, for all Q and I, Fig. 4 shows that $\overline{\Delta T}_{mid}$ is nearly independent of pressure in the continuum regimes (P > 5000 Pa). However, in the slip-flow rarefied regime, $\overline{\Delta T}_{mid}$ increases as the pressure decreases.

Model Validation NP program researchers constructed a geometrically accurate computational mesh of the experimental apparatus, including the heater rods, enclosure, spacer plates, and helium gas, and performed CFD simulations using ANSYS/Fluent [13]. In these simulations, the researchers employed the measured enclosure and spacer plate temperatures as boundary conditions. The simulations generated the measured total heat uniformly within the rods. The simulations modeled conduction in all solid components, and natural convection and radiation heat transfer across the gas.

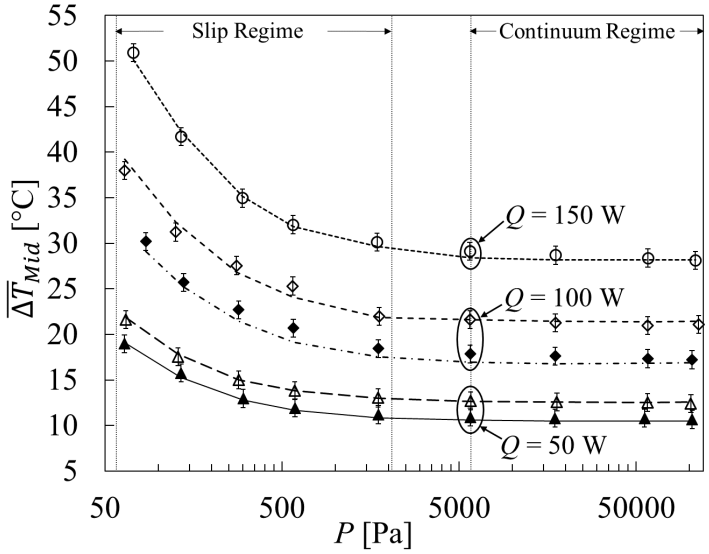

Figure 4: Measured (symbols) and simulated (lines) average mid-height temperature difference versus pressure for three heat generation. Open and solid symbols are for, respectively, I = 2.5 and 5.1 cm.

ANSYS/Fluent simulations model the helium as a continuum. However, under vacuum drying conditions, helium in the small passages of the cask is in the slip-flow rarefied gas regime [10]. In this regime, away from the wall, the gas is accurately modeled as a continuum. However, to model the effect of slip-flow rarefaction on heat transfer, we employ a user defined function to implement a heat flux thermal resistance $R_{TJ} = \frac{\zeta_T \lambda}{k}$ at all solid/gas interfaces. In this expression, k is the gas thermal conductivity near the surface and the mean free path between molecular collisions is $\lambda = \frac{T\mu_0}{P}\sqrt{\frac{2k_B}{mT_0}}$ [11]. The helium pressure and temperature are P and T, μ_0 is the gas dynamic viscosity at temperature T_0, m is the mass of the gas molecule, and k_B is Boltzmann's constant. The temperature jump coefficient ζ_T for monoatomic and polyatomic gases may be found from the gas/surface thermal accommodation coefficient α [14], and the gas Prandtl number Pr and specific heat ratio γ as $\zeta_T = \left(\frac{2-\alpha}{\alpha} + 0.17\right)\frac{\sqrt{\pi}\gamma}{(\gamma+1)\mathrm{Pr}}$ [15, 16]. These expressions show that both the mean free path and the slip flow thermal resistances increase as the pressure decreases.

Figure 5a shows the simulated vertical component of velocity w and temperature T in a plane near the experiment the mid-height, z = 0, for a simulation with Q =100 W, P = 112.7 kPa, and I = 2.54 cm [13]. The plane z = 0 passes through the simulated heater rods, helium gas, and enclosure. Figure 5a shows the temperatures of the solid and gas components are higher near the experiment centerline than near the enclosure. It also shows that the helium gas moves upward near the centerline and downward near the enclosure, and the rod velocities are zero (as they should be). The solid and dashed lines in Figure 4 show the simulated mid-height temperature difference $\overline{\Delta T}_{mid}$ for the same pressures, heat generation rates, and insulation thicknesses (wall temperatures) as the experiments. This plot shows that the simulated dependence of $\overline{\Delta T}_{mid}$ on these factors is very close to the measured dependence, including the effect of low-pressure rarefaction.

We define the local thermocouple-to-wall temperature difference ΔT as the value at the location of a rod thermocouple minus the minimum wall temperature. For each experiment (each I, Q and P), there is one thermocouple-to-wall temperature difference for each of the 49 rods. Figure 5b shows the simulated versus measured thermocouple-to-wall temperature difference (ΔT_{Sim} versus ΔT_{Mea}). It includes results

from the 25 experiments conducted in the slip-flow regime (below P < 5000 Pa), for both insulation thicknesses, and three heat generation rates (1225 data points). We observed that the simulated and measure thermocouple-to-wall temperature differences are highly correlated.

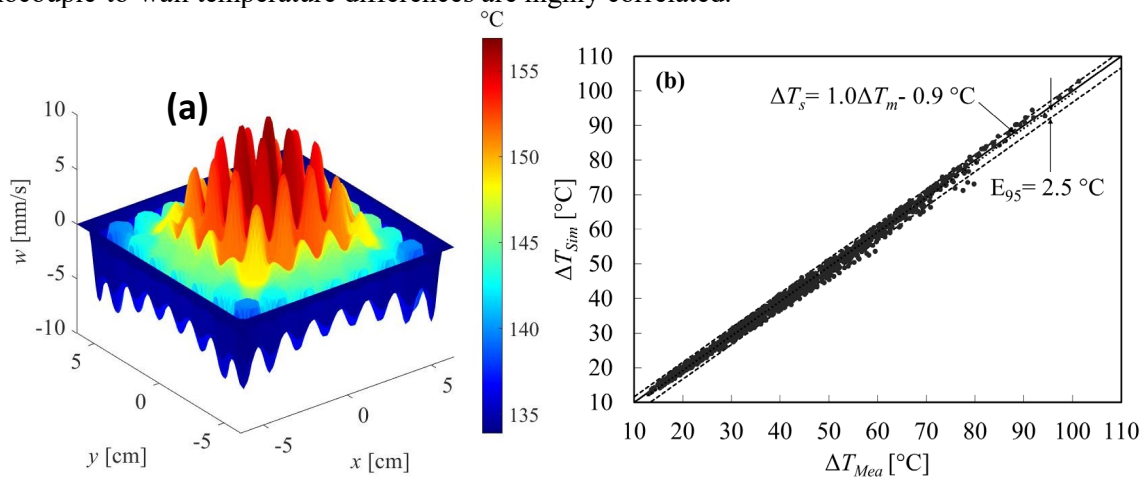

Figure 5 (a) Simulated vertical speed w and temperature at the experiment mid-height (z = 0) for $Q = 100\ W$, $P = 112.7\ kPa$, and $I = 2.54\ cm$. (b) Simulated versus measured rod-to-wall temperature differences for all measurement locations, heat generation rates, and insulation thickness in the slip rarefied-gas regime.

The solid line in Fig. 5b shows $\Delta T_{Sim} = \Delta T_{Mea}$. If the simulations perfectly recreated the experimental data, then all data would lie on that line. The dotted line in Fig. 5b (visible in the range $80°C < \Delta T_{Mea} < 100°C$) shows the least-squares linear best fit to the data, $\Delta T_{Mea,fit} = 1.0\Delta T_{Mea} - 0.9°C$. The dashed lines are above and below that dotted line by an amount that statistically contains 95% of the data (twice the standard estimate of the error [17]). This quantitative validation suggests that, on average, the simulations systematically under predict all measured thermocouple-to-wall temperatures differences by approximately 0.9°C. However, random differences between the simulations and experiments cause random differences in ΔT of about $E_{95} = 2.5°C$. A similar analysis comparing the simulated to the measured thermocouple-to-wall temperature difference for the 20 experiments in the continuum region (P > 5000 Pa) had 980 data points. It indicates that on average, the continuum simulations systematically underpredict the measured temperature by 0.6°C, and random difference cause 95% of the simulations to deviate from the best fit line by $E_{95} = 2.0°C$. The systematic and random errors in the rarefaction model are the reason its systematic and random errors are larger than those for the continuum simulations. These results show that the simulations accurately predicted the experimental temperatures in both the continuum and slip regimes.

CASK DRYING and STORAGE TEMPERATURE SIMULATIONS

In this section, we implement the simulation methods whose validation was described in the last section into two-dimensional models of the rail cask shown in Fig. 2 [7]. We used these simulations to predict the T_{PC} under normal vacuum drying, storage and transport conditions, for different basket/rail gap configurations. We consider the rail package in Fig. 2 because it contains more assemblies and would have higher steady-state temperatures than the truck package in Fig. 1. Our goal is to determine how the peak cladding temperature is affected by uncertainties in the basket/rail gap size (assuming the basket is centered but the gap is reduced due to thermal expansion), and nonuniformity (assuming the basket in Fig. 2 shifts to one side or diagonally).

In these simulations, each fuel assembly generates 950 W and is 3.66-m long, the heat generation rate in the plane under consideration is 10% higher than the average, the cask is filled with dry helium, and heat

transfer from the cask outer surface to a 24ºC-environment is by radiation and natural convection (modelled using appropriate emissivity and heat transfer coefficient values). During storage and vacuum drying, the domain in Fig. 2 is level, and so natural convection within the cask interior gaps is not modelled.

Continuum Conditions When the basket is centered within the cask, the top, bottom, and side basket/rail gaps in Fig. 2 are equal, with a nominal width of W = 4.78 mm. Based on the symmetry of this geometry and uniformity of the heat generation and boundary conditions, we expect the cask temperature field to exhibit symmetry about horizontal, vertical, and diagonal lines that pass through the center of the cask in Fig. 2. To take advantage of this symmetry, we employ a pie-shaped computational mesh with symmetry boundary conditions imposed on the radial symmetry edges (see Fig. 6a). This mesh is one-eight as large as the full domain shown in Fig. 2. Because thermal expansion may reduce this basket/rail gap by unknown amounts and may affect the predicted peak cladding temperature, we consider gap widths of W = 0, 1.27, 2.54, and 4.78 mm. To model different basket/rail gap widths, we increase the thicknesses of the stainless-steel skin that wraps around the basket.

Figure 6a shows the temperature contours within the pie-shaped domain for the nominal gap width W = 4.78 mm, for helium in the continuum regime (P = 220 kPa) [7]. The hottest location is in the central fuel assemblies and is shown using a five-pointed star. The predicted peak cladding temperature is $T_{PC} =$ 273℃. In Figure 7, the solid triangles connected with solid lines show the peak clad temperature for basket/rail gap average widths of W_{AVG} = 0, 1.27, 2.54, and 4.78 mm (for this configuration, the gap width is uniform, so the average gap width is $W_{AVG} = W$) [7]. We see that in the continuum regime, reducing the basket rail gap width from 4.78 to 0 mm reduces the predicted T_{PC} by 48℃. This indicates that the realistic uncertainty of the basket/rail gap leads to significant uncertainty in the peak cladding temperature.

To quantify the effect of the basket *shifting* relative to the rest of the cask, we constructed two additional computational domains. In one case, the basket is shifted to the right in Fig. 2, such that it touches the rails on the right, the gap width on the left is double to 9.56 mm, and the top and bottom gaps are the nominal value. In this case, the geometry is symmetric about a horizontal line passing through the center of Fig. 2. In the other case, the basket is shifted diagonally to the right and upward, so the upper and right basket surfaces in Fig. 2 touch the rails, but the gaps on the bottom and left are twice the nominal value. In this case, the geometry is symmetric about a diagonal line that passes through the center of Fig. 2, from the lower left to the upper right. In both shifted simulations, we assume the basket does not expand, and so the *average* gap width is the same as the nominal value, $W_{AVG} = 4.78\ mm$. Figures 6b and 6c show the resulting temperature contours for a continuum pressure of P = 220 kPa (symmetry is imposed along the radial surfaces of these domains) [7]. The five-pointed stars show the hottest locations. When the basket is shifted to the right, compared to the centered basket with the nominal gap width, the peak cladding temperature decreases by 7℃. When it is shifted diagonally, such that two of the basket surfaces are in direct contact with the rails, the peak cladding temperature decreased by 10°C. These peak clad temperatures are shown in Figure. 7 using open triangles connected by dotted lines at W_{AVG} = 4.78 mm. While shifting reduces the cladding temperature compared to the centered basket with the nominal spacing, the reduction is not as large as the reduction caused by completely closing the gap.

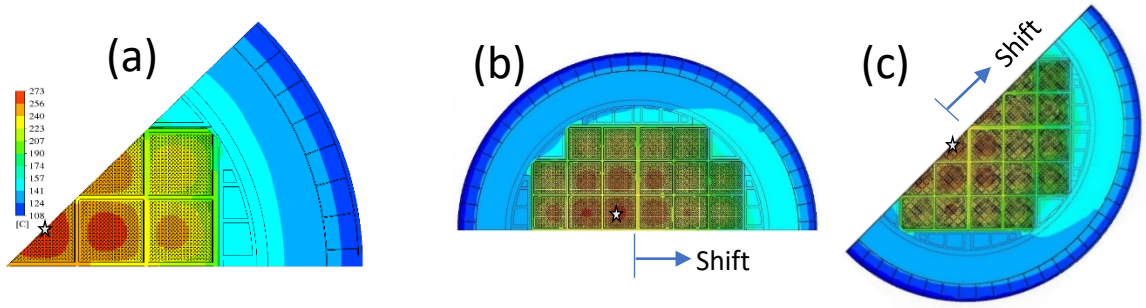

Figure 6: Two-dimensions SNF cask cross-section continuum simulation results, with average gap widths of $w_a = 4.78\text{-}mm$. Five pointed stars indicate the hottest locations. (a) Centered basket. (b) Basket shifted to the right. (c) Basked shifted diagonally.

Rarefied Conditions Figure 7 includes comparable simulation results for rarefied gas conditions at P = 400 Pa (solid and open diamonds) and P = 100 Pa (solid and open squares) [7]. At these low pressures, decreasing the pressure increases the T_{PC} for all gap widths, both with and without shifting. This is because rarefaction decreases conduction through the helium gas at the gas-solid interfaces. As described earlier, this effect is particularly strong in the basket/rail gap because the heat transfer rate across the gap is large and radiation heat does not significantly contribute to heat transfer. Rarefaction has a much smaller effect on the peak cladding temperature if the basket/rail gap is eliminated (see W = 0). Under that condition, conduction heat transfer from the fuel assembly rods to the surrounding basket tubes is reduced. However, since the temperature of that region is relatively high, heat is also transferred by radiation. As a result, the reduction in conduction caused by rarefaction is not as important for W = 0 as it is for finite gap widths. For P = 400 and 100 Pa, reducing the basket rail gap width from 4.78 to 0 mm reduces the predicted peak cladding temperature by, respectively 60℃ and 78℃. The open squares and diamonds show how the peak cladding temperatures decrease when the basket is shifted. Once again, the effect of basket shifting is not as significant as eliminating the gap.

The results in Fig. 7 show that the uncertainty in the peak cladding temperature caused by uncertainty in the gap configuration is larger in the slip-flow rarefied gas conditions than it is in the continuum regime. Currently, steady-state fuel assembly temperatures are being measured in a TN32 cask for a variety of pressure conditions [18]. In the future, these measurements will be used to validate geometrically accurate three-dimensional simulations of the cask. However, the size and uniformity of the experimental basket/rail gap size are unknown. The current results will be used to determine how much these unknown gap dimensions can affect the peak cladding temperature. This can be used to determine if the simulation results are close enough to the measurements.

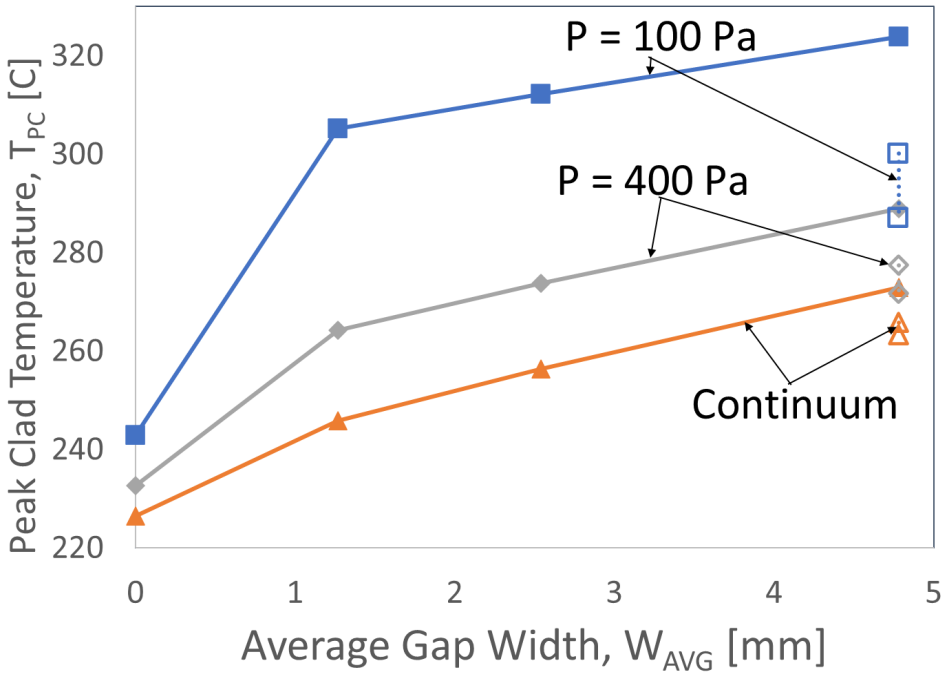

Figure 7: Simulated steady-state peak clad temperature versus average gap width for three helium-filled cask internal pressures. Solid symbols show centered basket results. The hotter open symbols show results with the basket shifted to one side (Fig. 6b). The lower open symbols show results with the basket shifted diagonally (Fig. 6c).

FIRE MODEL DEVELOPMENT

NP Program researchers worked with Sandia National Laboratories to conduct two series of large-scale fire tests to measure temperatures of massive carbon-steel pipe calorimeters engulfed in jet-fuel fires, for a range of calorimeter sizes and wind conditions [19, 20]. The goal of those tests was to acquire data to validate CFD/radiation heat transfer fire simulation codes that predict heat transfer from fires to massive objects.

In one test series of tests, a 2.4-m-diameter, 4.6-m-long, 2.54-cm thick carbon-steel calorimeter is centered above a 7.9-m-diameter pool containing 7.57 m^3 (2000 gallons) of JP4 jet fuel. The bottom of the calorimeter was 1 m above the pool. These conditions are consistent with federal regulations regarding HAC fire tests [2]. Fifty-eight thermocouples were strap welded to locations distributed over the calorimeter body and end caps. The calorimeter temperatures, temperatures of foil radiant heat flux gages at several locations near the calorimeter, and wind conditions were measured as functions of time during three fire test that were performed using this configuration [20].

In both Tests 1 and 2, the average wind speed was approximately 1 m/s, the fuel was consumed in around 40 minutes, and the calorimeter was mostly engulfed in flames. Figure 8a shows the typical level of engulfment. In Test 3, the average wind speed was approximately 3.5 m/s, and the fuel was consumed in 25 minutes. As shown in Fig. 8b, the wind tilted the flames and reduced the calorimeter's engulfment compared to Tests 1 and 2. A very strong recirculation zone formed on the leeward end of the calorimeter. The foil radiate heat flux gages indicated the temperatures in that region were hotter than other regions of the flames.

The solid lines in Fig. 9 show the average calorimeter internal-surface temperature versus time for all three tests. The average temperature rise is a good indication of heat transfer from the fire to the calorimeter. The measured average temperatures are very similar in Tests 1 and 2, and both are substantially hotter than

the Test 3 temperatures. This difference is because the calorimeter was more engulfed during Tests 1 and 2 than during Test 3.

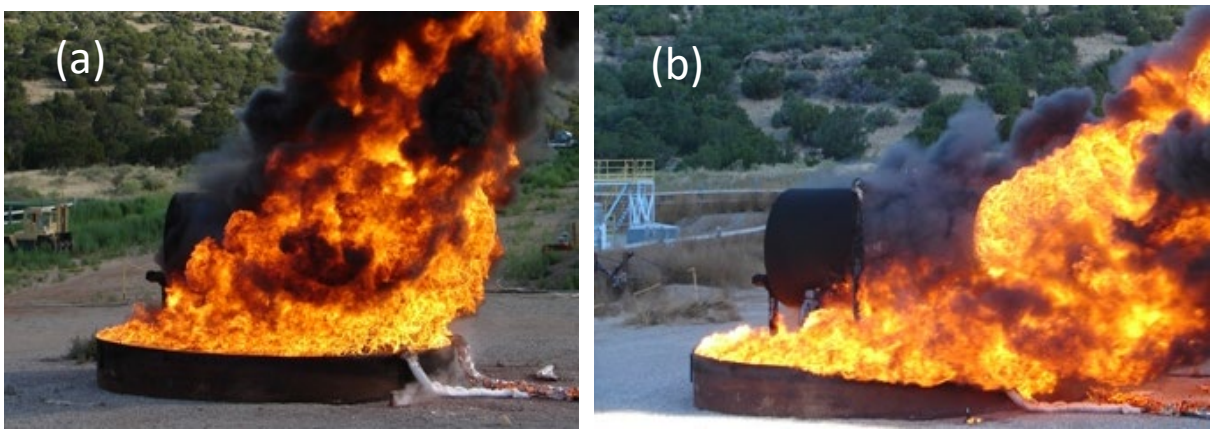

Figure 8: A 2.4-m-diameter, 4.6-m-long, 2.54-cm thick carbon steel calorimeter whose lowest surface is centered 1 m above a 7.9-m-diameter pool containing 7.57 m^3 of JP4 jet fuel. (a) Flames during the moderately low speed wind conditions which existed in Tests 1 and 2. (b) Flames during Test three with stronger winds than Test 1 and 2.

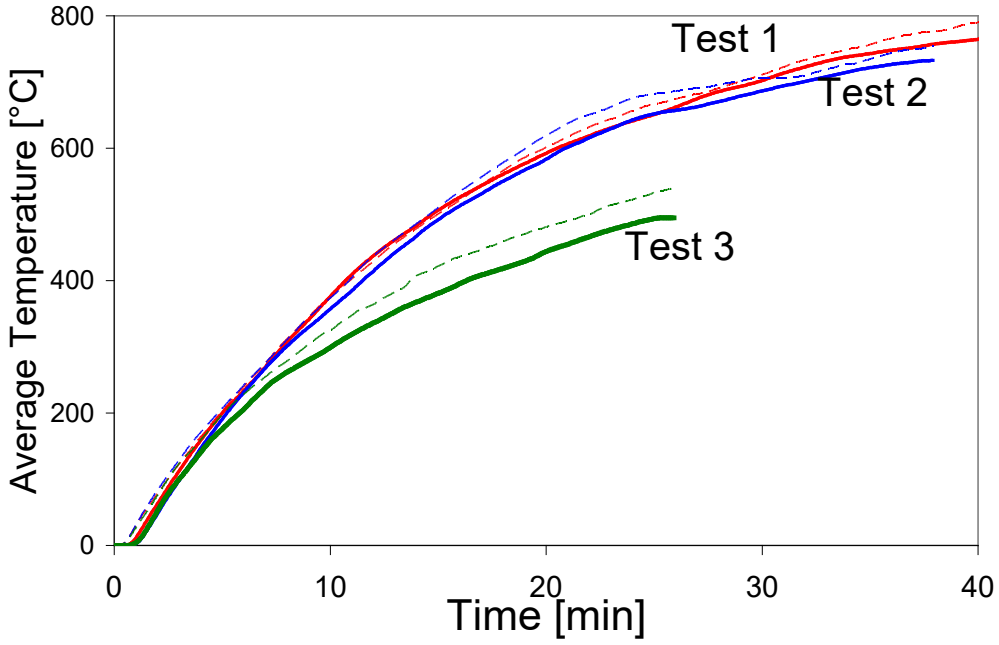

Figure 9: Average measured (solid lines) and simulated (dashed lines) calorimeter temperatures versus time during fire Test 1, 2 and 3.

C3d is a fully functional CFD code [21]. It employs the Rosseland conduction approximation to model radiation heat transfer in highly sooty fires, which are characterized by high media absorption and short absorption lengths. This approximation employs an effective, temperature-dependent thermal conductivity of the flowing medium equal to $k_R = 16\sigma n^2 T^3/3\beta_R$. In this expression, T is the local temperature, σ is the Stephan-Boltzmann constant, β_R is the local extinction coefficient of the medium, and n is the media index of refraction. C3d calculates the local extinction coefficient as a function of the local mass fractions

of soot, water vapor, fuel vapor and intermediate species. At typical fire temperatures and species concentrations the Rosseland conductivity is much larger than the molecular value for air. The NP Program researchers worked with Computational Engineering Analysis LLC to use the calorimeter fire test data to adjust and validate physics-based models within the *C3d* CFD/radiation heat transfer simulations [19, 22].

NP Program researchers constructed a three-dimensional rectangular domain of the fire tests. For each test, they applied the measured wind conditions to its four sides, pressure outlet conditions to it top, and no slip conditions to most of its floor. They modeled the fuel basin and calorimeter, and injected fuel from the basin surface at the measured fuel consumption rate. The researchers linked the fire model to a model of the calorimeter and monitored the temperatures at the locations of its 58 interior surface thermocouples. The dished lines in Fig. 9 show the average of the simulated interior surfaces. Comparing the simulation results with the measure data (solid lines) shows good qualitative agreement for a range of wind conditions. Computational Engineering Analysis and the NP Program have validated C3d against a wide variety of other relevant large fire tests [23, 24]. These successful validation efforts support the use of C3d to predict the response of SNF transport packages under severe accident conditions.

CASK FIRE TEMPERATURE SIMULATIONS

The NP Program researchers investigated the response of the legal-weight truck package in Fig. 1 to a range of fire conditions [4, 25, 26]. They employed this smaller package because its temperatures rise faster during a fire, and its components may reach their temperatures of concern more quickly, than the larger rail package in Fig. 2.

The researchers constructed a finite element thermal model of the truck package and linked it to a C3d fire simulation domain. The fire domain sides were 40-m long and 12-m high and had a ground level fuel pool at the center. Pressure boundary conditions were imposed on the domain sides and top to model a no-wind conditions. The lowest surface of the cask model was 1 m above the domain floor. In the linked system, the fire model calculates the spatially varying heat transfer from a fire to an engulfed package for a given package surface temperature profile. The package model then calculates the package temperature response to the fire heat transfer and updates the package surface temperature. The linked package and fire models run alternately until the time dependent fire simulation is complete.

Initial simulations with the cask centered over the pool were performed for a range of pool diameters. These simulations determined that the minimum diameter that substantially engulfed the cask and its impact limiters in flames (as specified in [2]) was 12-m. This pool diameter was used in all subsequent simulations. However, the 12-m pool diameter extends 2.9-5.5 m from the edges of the package. This is considerably more than the 1-3 m specified in the Code of Federal Regulations [2].

Federal regulations require that transport packages provide their required functions after a 30 minute fully engulfing fire. The objective of this study [4] was to predict the fire duration of concern for the fuel cladding. This is the minimum fire duration predicted to cause the fuel cladding to reach its burst rupture temperature, $T_{BR} = 750^oC$ [27]. We wish to determine this duration when package is centered over the fire ($S_X = 0$) and when it is offset from the center by different amounts, $S_X = 1.9, 3.4, 3.9, 4.4, 5.4$ and $6.4\ m$. We also wish to determine the safe distance. This is the minimum offset between the package and fire centers for which the cladding would not reach its limit temperature, no matter how long the fire lasts.

In this study, all simulations were performed with lowest surface of the package body 1-m above the domain floor. Figure 10a and 10b show snapshots of simulated transient fire surface temperature results for $S_X = 0$ (in which the package is fully engulfed in flames) and 6.4 (in which the package is partially unengulfed) [4]. Figure 10c shows the simulated peak fuel temperature versus time for all seven package locations. It includes a horizontal line for the potential cladding burst rupture temperature, $T_{BR} = 750^oC$. If the package is centered over the fire, the simulations predict that the peak cladding temperature rises relatively quickly and will reach its limit approximately 12 hours after fire ignition. As S_X increases, the fuel temperature increases more slowly, and fire duration of concern increases. For $S_X = 6.4\ m$ the peak cladding temperature appears to plateau at around t = 25 hours at approximately 550°C. This suggests that if the package center is further from the fire center than this safe distance, the cladding will not reach its

limit temperature, no matter how long the fire lasts. In this case, the safe distance is roughly equal to the 6 m radius of the fuel pool.

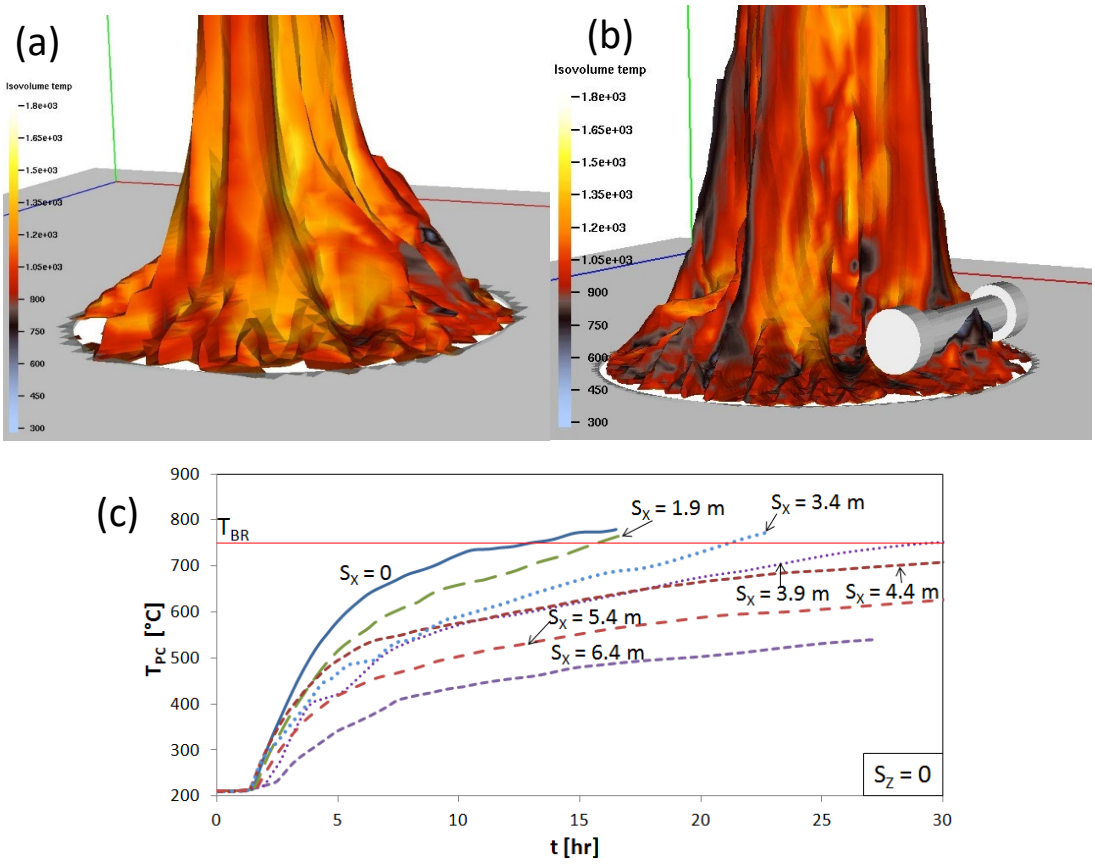

Figure 10: Regulatory format fire simulation results for a 12-m diameter jet fuel pool. (a) Flame surface temperature contours engulfing a truck cask centered 1 m over the pool ($S_X = 0$). (b) Flame surface temperature contours with the cask shifted $S_X = 4.4$ m away from the pool center. (c) Simulated peak clad temperature versus time for different cask-to-pool center distances, S_X. The cladding burst rupture temperature T_{BR} is included.

This study also monitored the temperatures of the package seal, gamma and neutron shield, and other components, and compared them to their limit values [4]. This type of analysis, in which the fire duration of concern and safe distance are determined for a range of fires, can be used by transportation risk analysis. It helps analysts distinguish between fire accident scenarios that potentially challenge the integrity of a transport package, and require additional and more detailed analyses, from scenarios that do not.

SUMMARY

Spent Nuclear Fuel (SNF) is dried, stored and transported in thick-walled packages. The temperatures of SNF package components affects their degradation rates. To assure SNF can be safely transported and processed after long term storage, as well as protect the public and environment after severe fire accident conditions, component temperatures must be accurately predicted to assure they do not exceed specified limits. Since 1993, researchers from the University of Nevada, Reno Nuclear Packaging Program have partnered with others to develop and experimentally validate computational fluid dynamics models to accurately predict temperatures in SNF casks under normal and severe fire accident conditions. This includes conducting experiments that simulate a SNF assembly within a package basket tube under normal storage/transport and vacuum drying conditions. They used these results to validate computational fluid

dynamics simulations for both continuum and slip-flow rarefied gas condition. They used the validated simulations to predict the effect of uncontrolled gap widths within a cask on the peak cladding temperature. Future work will use these methods to develop methods to validate geometrically accurate three-dimensional CFD simulations that predict package temperatures.

The NP Program worked with Sandia National Laboratories to conduct series of large-scale fire tests to measure heat transfer from jet fuel fires to engulfed objects for a range of object sizes and wind conditions. They worked with Computational Engineering Analysis LLC to use those data to validate the C3d CFD/radiation heat transfer fire code. They then used C3d to predict the fire duration of concern that could cause the fuel cladding and other components to reach their temperatures of concern. This type of analysis can be used to assess the potential risks of large-scale transportation campaigns.

REFERENCES

1. Saling, J.H., and Fentiman, A.W., 2017, Radioactive Waste Management, 2nd edition, Routledge, New York, 352 pages.
2. US Nuclear Regulatory Commission, 2011, 10CFR 71, “Packaging and Transportation of Radioactive Material,” Code of Federal Regulations.
3. NRC Docket Number 71-9225, NACLWT Legal Weight Truck Cask System Safety Analysis Report, June 2005, Rev. 37, Nuclear Assurance Corporation International, Norcross, Georgia, U.S.A.
4. Mittal, K., Greiner, M., Suo-Anttila, A.J., 2015, “Dependence of Fire-Time-of-Concern on Location of a One-Assembly Transport Package,” Nuclear Technology, Vol.192, pp. 142-154.
5. Kamichetty, K.K., Venigalla, V., and Greiner, M., 2014, “Development, Use, and Accuracy of a Homogenized Fuel Region Model for Thermal Analysis of a Truck Package Under Normal and Fire Accident Conditions,” Journal of Pressure Vessel Technology, Vol. 136/021208-1-12.
6. "TN-32 Final Safety Analysis Report (FSAR), Revision 2," Virginia Electric and Power Company, 2002.
7. Higley, M, … conference presentation or EPRI report/presentation ???
8. U.S. NRC, "Cladding considerations for the transportation and storage of spent fuel," ISG-11, Rev. 3, 2003.
9. W. Large, "Review of drying methods for spent nuclear fuel," Savannah River Site (US), 1999.
10. Hadj-Nacer, M., T. Manzo, M. T. Ho, I. Graur and M. Greiner, 2016 “Effects of Gas Rarefaction on Used Nuclear Fuel Cladding Temperatures during Vacuum Drying,” Nuclear Technology, 194, 3, pp: 387-399.
11. Bird, G., 1994, "Molecular Gas Dynamics and the Direct Simulation of Gas Flows (Oxford Engineering Science Series)," Clarendon, 1994.
12. Maharjan, D., M. Hadj-Nacer, and M. Greiner, 2020, “Temperature Measurement of a Heated Rod Array within a Square Cross Section Enclosure Filled with Dry Rarefied Helium,” International Journal of Heat and Mass Transfer, 148, 119033.
13. Maharjan, D., M. Hadj-Nacer, and M. Greiner, 2020, “Implementation and Experimental Validation of a Computational Model to Predict Temperatures and Heat Transfer of a Square Array of Heated Rods Enclosed in a Pressure Vessel Filled with Rarefied Dry Helium,” International Journal of Heat and Mass Transfer, 158 (2020) 120050.
14. S. Song and M. Yovanovich, "Correlation of thermal accommodation coefficient for engineering surfaces," ASME HTD, vol. 69, pp. 107-116, 1987.
15. Lin, J.T. and D. Willis, "Kinetic theory analysis of temperature jump in a polyatomic gas," The Physics of Fluids, vol. 15, no. 1, pp. 31-38, 1972.
16. M. Hadj-Nacer, D. Maharjan, M.-T. Ho, S. K. Stefanov, I. Graur, and M. Greiner, "Continuum and kinetic simulations of heat transfer trough rarefied gas in annular and planar geometries in the slip regime," Journal of Heat Transfer, vol. 139, no. 4, 2017.
17. Wheeler, A.J. and Ganji, A.R., 2010, Introduction to Engineering Experimentation, 3rd Edition, Prentice Hall.

18. Hanson, B., "High Burnup Spent Fuel Data Project & Thermal Modeling and Analysis," in NWTRB Meeting, Albuquerque, NM, 2018.
19. Kramer, M.A., Greiner, M., Koski, J.A. Lopez, C., and Suo-Anttila, A., 2003, "Measurements of Heat Transfer to a Massive Cylindrical Object Engulfed in a Circular Pool Fire," J. Heat Transfer, Vol. 125, pp. 110-118, 2003.
20. Greiner, M., del Valle, M., Lopez, C., and Figueroa, V., 2013, "Thermal measurements of a rail-cask-size pipe-calorimeter in jet fuel fires," Journal of Fire Protection Engineering, 2013.
21. Suo-Anttila, A., Lopez, C., and Khalil, I., 2005, User Manual for CAFE-3D: A Computational Fluid Dynamics Fire Code, SAND2005-1469.
22. del Valle, M.A., Kramer, M.A., Lopez., C., Suo-Anttila, A., and Greiner, M., 2007, "Temperature Response of a Rail-Cask-Size Pipe Calorimeter in Large-Scale Pool Fires," proceedings of the 15th International Symposium on the Packaging and Transportation of Radioactive Materials (PATRAM).
23. Greiner, M., and Suo-Anttila, A., 2004, "Validation of the ISIS Computer Code for Simulating Large Pool Fires Under a Varity of Wind Conditions," ASME J. Pressure Vessel Technology, Vol. 126, pp. 360-368.
24. Greiner, M., and Suo-Anttila, A., 2006, "Radiation Heat Transfer and Reaction Chemistry Models for Risk Assessment Compatible Fire Simulations," Journal of Fire Protection Engineering, Vol. 16, pp. 79-103.
25. Chalasani, N.R., Greiner, M., and Suo-Anttila, A., 2012, "Benchmarking of Container Analysis Fire Environment simulation using the memorial tunnel fire ventilation tests," Journal of Fire Protection Engineering, 22(1) 45–70.
26. Greiner, M., Chalasani, N.R., and Suo-Anttila, A, 2011, "Simulated Response of a One-PWR Truck Package to the Caldecott Tunnel Fire Scenario," paper 11573, Waste Management Symposium (WM2011), February 27- March 4, Phoenix, AZ.
27. Sprung, J. L., Ammerman, D. J., Breivik, N. L., Dukart, R. J., Kanipe, F. L., Koski, J. A., Mills, G. S., Neuhauser, K. S., Radloff, H. D., Weiner, R. F., Yoshimura, H. R., 2003, Reexamination of Spent Fuel Shipment Risk Estimates, NUREG/CR-6672, Volume1, Sandia National Laboratories, Albuquerque.